Atmos. Chem. Phys. Discuss., 5, 10019–10053, 2005
www.atmos-chem-phys.org/acpd/5/10019/
SRef-ID: 1680-7375/acpd/2005-5-10019
European Geosciences Union

Atmospheric Chemistry and Physics Discussions

Modeling atmospheric CO_2 concentration profiles and fluxes above sloping terrain at a boreal site

T. Aalto[1], J. Hatakka[1], U. Karstens[2], M. Aurela[1], T. Thum[1], and A. Lohila[1]

[1]Climate and Global Change Research, Finnish Meteorological Institute, P.O. Box 503, 00101 Helsinki, Finland
[2]Max Planck Institute for Biogeochemistry, P.O. Box 100164, 07701 Jena, Germany

Received: 30 August 2005 – Accepted: 13 September 2005 – Published: 14 October 2005

Correspondence to: T. Aalto (tuula.aalto@fmi.fi)

Abstract

CO_2 fluxes and concentrations were simulated in the planetary boundary layer above subarctic hilly terrain using a three dimensional model. The model solves the transport equations in the local scale and includes a vegetation sub-model. A WMO/GAW background concentration measurement site and an ecosystem flux measurement site are located inside the modeled region at a hilltop and above a mixed boreal forest, respectively. According to model results, the concentration measurement at the hill site was representative for continental background. However, this was not the case for the whole model domain. Concentration at few meters above active vegetation represented mainly local variation. Local variation became inseparable from the regional signal at about 60–100 m above ground. Flow over hills changed profiles of environmental variables and height of inversion layer, however CO_2 profiles were more affected by upwind land use than topography. The hill site was above boundary layer during night and inside boundary layer during daytime. The CO_2 input from model lateral boundaries dominated in both cases. Daily variation in the CO_2 assimilation rate was clearly seen in the CO_2 profiles. Concentration difference between the hill site and the forest site was about 5 ppm during afternoon according to both model and measurements. The average modeled flux to the whole model region was about 40% of measured and modeled local flux at the forest site.

1. Introduction

Transport of CO_2 in the atmosphere has been studied by several methods including 3-D atmospheric modeling based on existing climate models and vegetation models suitable for regional or global scale studies (e.g. Knorr and Heimann, 2001; Chevillard et al., 2002; Kjellström et al., 2002; Dargaville et al., 2002; Chan et al., 2004; Geels et al., 2004; see also Gurney et al., 2004, for connection with inversion studies), single measurement site based modeling of concentrations and footprints using K-theory for

ACPD

5, 10019–10053, 2005

turbulence and an accurate description of the vegetation (Sogachev et al., 2002; Denning et al., 2003), and Lagrangian footprint modeling, which, in addition to accurate flux source determination, can produce concentration footprints upwind from measurement towers (e.g. Rannik et al., 2000; see also Vesala et al., 2004).

Studies of mountainous regions are important, because many sites are situated on a sloping terrain or there are hills nearby that may distort the atmospheric distribution of transferring species and turbulent wind fields by e.g. creating local changes in energy balance, mountain waves and venting of atmospheric layers. These effects have been studied in mountainous environments by e.g. Grell et al. (2000), Carvalho et al. (2002), Henne et al. (2004) and Turnipseed et al. (2004) and for mountainous Iberian coastline by Gangoiti et al. (2002). Flux footprint modeling has also been extended to complex sites (e.g. Rebmann et al., 2005; Sogachev et al., 2005).

Accurate tropospheric CO_2 concentrations are often measured in elevated sites, on top of mountains or towers to obtain a good representability in regional scale. Monitoring of fluxes, however, is made above flat, homogeneous surface, which often corresponds to low altitude measurement based on a separate site. There is at least one order of magnitude difference in the concentration and flux footprints (e.g. Gloor et al., 2001; Denning et al., 2003). The concentration measurement is, however, effected to some extent by the local fluxes, and studies at sites where both concentrations and fluxes are measured are interesting from the point of view of clarifying the actual source patterns and representativeness of the concentration measurement with the help of local sink variation. Besides high altitude concentration measurement, similar analysis for concentrations at the flux tower height is useful in considering possibilities for concentration measurement on flux towers.

The link between regional modeling and point measurements is important because regional scale models can not resolve all the details in challenging heterogeneous sites. For forward and inversion modeling it is essential to know how local concentration measurements should be interpreted and flagged, and how local sinks can be generalized to a larger region (Ramonet and Monfray, 1996; Turner et al., 1996;

ACPD
5, 10019–10053, 2005

Houweling et al., 2000). A straightforward way to address these issues is to build a local scale model, connect it to regional scale model and validate it with continuous high frequency concentration and flux measurements.

This study combines modeling of CO_2 vegetation fluxes and 3-D atmospheric CO_2 profiles, meteorological fields and heat fluxes above a complex terrain in a local scale using realistic lateral boundary forcing. The objective is to find out how much the high altitude concentration measurement is influenced by local sinks and sources during the course of a day in comparison to the regionally modeled concentration in the free troposphere, and how representative a concentration measurement would be at the flux tower height. Sink estimates are made for the model domain covering 100 km^2 and compared to point estimate from the flux measurement site.

2. Materials and methods

2.1. Measurements

Measurements were made at Pallas-Ounastunturi National park in northern Finland in a sparsely populated region (<2 inhabitants km^{-2}). The distance to nearest village (Muonio) of 2500 inhabitants is about 19 km. The site is located at the northern limit of the boreal forest zone in continental region. Distance to the Atlantic ocean coastline is about 300 km. The location above the Arctic circle corresponds to polar night lasting for about three and half weeks in winter and polar day lasting for seven weeks in summer. The climate is subarctic with monthly mean temperatures of about −11°C in February and 13°C in July. The annual average for years 1996–2004 is −1.1°C. The ground is covered with snow from October to May.

Concentrations were measured at the top of Sammaltunturi hill (67°58′24″ N, 24°06′58″ E, 565 m above sea level, hereafter 'hill site'), see Fig. 1. The sparse ground vegetation consists of low vascular plants, mosses and lichens among partly revealed bedrock. The treeline is about 100 m below the station altitude. The site is surrounded

ACPD
5, 10019–10053, 2005

by other hills, forests, wetland patches and small lakes. The inlet for the CO_2 sampling line was located 10 m above ground at the roof of the station building. CO_2 was measured as a mean of one minute sampling 12 times in an hour with Li-Cor 6252 NDIR infra-red gas analyser. The measurement was calibrated once in every 2.5 h against three working standard gases (about 330 ppm–380 ppm). In addition, a reference gas with concentration of 318 ppm was measured every 7.5 h. These gases were calibrated every three months against WMO/CCL (NOAA) standards. The measurements are described in detail in Hatakka et al. (2003).

Fluxes of CO_2, water and heat were measured by eddy covariance (EC) technique at Kenttärova (67°58′ N, 24°14′ E, 310 m a.s.l., hereafter 'forest site') during July 1998. The distance to the Sammaltunturi top was about 5 km (see Fig. 1). The site was constructed on mixed forest consisting of Scots pine (Pinus sylvestris), Norway spruce (Picea abies) and downy birch (Betula pubescens). The measurement height at the tower was 18 m above ground while the surrounding trees were about 13 m tall. Later during year 2002 the eddy flux measurements were started above old growth spruce forest about 2 km away (67°59′14″ N, 24°14′36″ E). These measurements are not considered here (spruce forest covers less than 9% of the total modeled region), it is just noted that the overall level and daily cycle of the fluxes is rather similar to the older site. The eddy covariance instrumentation included a three-axis sonic anemometer (ATI SWS-211) and Li-Cor 6262 NDIR infra-red closed path CO_2/H_2O analyser. Concentration readings from the eddy covariance system were also utilized. They have an accuracy of about 3 ppm, much lower than hill top where an accuracy of 0.1 ppm was attained. For details see Hatakka et al. (2003).

Soil chamber measurements were also performed at the top of Sammaltunturi hill to examine the influence of ground vegetation CO_2 fluxes on the concentration measurement. Several plots were chosen where land cover varied from partly revealed rock (quartzite) surface to dense population of mosses, lichens and low vascular plants. Steady state CO_2 and transpiration fluxes were measured in near-optimal temperature and saturating irradiance using a plastic soil chamber together with infrared gas

analyzer to measure the changes in CO_2 concentration.

2.2. Model

2.2.1. Grid and land use

The model domain was built using the commercial grid generator Gambit. Site topography and land cover data from Finnish Land Survey (Fig. 1) were inserted to the model, and a grid was constructed to describe the boundary layer above the site. The size of the model domain is 10 km in horizontal and 3 km in vertical direction. The grid consists of tetrahedral elements. The shape and size of grid elements was adapted by the grid generator to best fit the topography, while the faces of the elements coinciding with the ground surface were always of square shape with a resolution (i.e. side length) of 50 m. A narrow soil layer of 5 cm thickness was inserted as an additional wall conduction zone to the ground surface. The heat conduction properties of the layer were those typical to moist peat soil and water for lake surfaces.

Land cover data was divided into four forest classes according to tree density, originally reported in 25 m accuracy (Table 1). Corresponding leaf area indexes were estimated using experimental data from northern Finland. The fifth class was reserved for wetlands and the sixth for lakes. Open wetlands were present at a significant proportion in the surrounding region but they covered less than 5% from the current model domain, owing to its mountainous character. The forest in the modeled region was dominated by about 37% of mixed species and by 63% of single species. Of the latter, 84% were Scots pine, 15% Norway spruce and less than 1% downy birch dominated forests. Forest classes were divided according to tree density rather than species, since mixed forests covered a significant portion of the domain region and the flux measurements considered here were made above mixed forest (of which the largest proportion was pine). Surface roughness values for momentum and heat for forest, grassland and lakes were taken from literature (Troen and Petersen, 1989; Beljaars and Holtslag, 1991; Wieringa, 1992).

ACPD
5, 10019–10053, 2005

2.2.2. Solver

Fluxes and concentrations were solved using the commercial code Fluent© utilizing finite element methodology. Energy, turbulence, fluid and species transport equations were solved in segregated mode. Surface exchange formulations and boundary conditions were programmed as user defined C codes and inserted to the basic simulation system.

Inputs at the model lateral boundaries (air temperature, humidity, wind components, pressure, total water column) were obtained from ECWMF MARS database and inputs for CO_2 from the regional model REMO (Chevillard et al., 2002) covering the Eurosiberian region with a 0.5 degree grid resolution. Meteorological values were forced to externals at boundaries, which resulted in about 500 m transition region near the boundary.

The surrounding terrain consisted of a similar mosaic of forest and wetlands than the site itself and it was relatively flat especially in the prevailing wind direction. Thus, large scale influences to fluid stream patterns and heat fluxes that might not be resolved in the input data were not expectable.

The model was non-hydrostatic, i.e. pressure changes were allowed in addition to the meteorological input pressure. Turbulence inside the domain was simulated with standard K-epsilon theory. Turbulent kinetic energy and dissipation rate input at model boundaries were calculated according to Rao and Nappo (1998).

2.2.3. Radiation and heat balance

Absorption and scattering of radiation in air was simulated for shortwave and near infrared wavelengths, respectively. Water vapour is the most significant absorber in the lower troposphere lowering the heating rate in the near infrared region by about 10 W m^{-2} at the lowest 3 km according to line parametrization by Chou (1992), adapted to current Pallas conditions. Absorption by other constituents did not change the simulation result significantly, and thus they were neglected to save computational time.

ACPD
5, 10019–10053, 2005

Radiation at the surface was obtained from local measurements and the total potential global radiation at the surface was modeled according to Savijärvi (1990). Radiation in other altitudes was modeled according to NIR line absorption of water vapour. The simulated day was clear and thus cloud parametrizations were not applied.

Surface heat balance was calculated for each surface grid cell. The incoming shortwave radiation is balanced by surface longwave radiation, and latent, sensible and ground heat fluxes (e.g. Hartmann, 1994). Incoming radiation is partly absorbed and partly reflected. Shortwave albedo and longwave emissivity for the site was obtained from MODIS satellite observations as an average of high growing season values since data from 1998 was not available. Atmospheric stability was formulated through Monin-Obukhov similarity theory (e.g. Kaimal and Finnigan, 1994). Details of heat exchange calculations are given in the Appendix A.

2.2.4. Gas exchange by the surface

The complexity of the vegetation model (see Appendix A) is adjusted so that it covers the main features of the site while simultaneously maintaining reasonable simulation time in connection with the atmospheric transport model, which is densely gridded due to the complex topography, and thus computationally expensive. The goal was to provide realistic estimations of surface fluxes for examining the atmospheric concentration profiles.

The forest canopy was divided into four layers according to the distribution of leaf area index in the canopy. Each layer was treated separately for CO_2 exchange and conductance calculations. Fluxes and conductances were further divided into sunlit and shaded portions depending on the incoming PAR irradiance. Irradiance at different layers was simulated according to a two-way approximation by Sellers (1985), see also Sellers et al. (1996).

CO_2 fluxes of a single leaf inside a canopy layer were simulated according to principles by Farquhar et al. (1980). The gas exchange rate is limited by Rubisco activity or RuPB regeneration rate, and CO_2 concentration, temperature and irradiance are

considered to be the key driving environmental variables in the leaf CO_2 exchange simulation. The conductance of the leaf was simulated according to Ball et al. (1987). Local flux data was used in fitting of parameters of the conductance equation, again dependent on CO_2 assimilation rate, relative humidity (RH) and CO_2 concentration.

To obtain the total canopy exchange rate, assimilation and respiration fluxes at each layer were added together and the soil respiration rate was subtracted from the sum. Soil respiration was obtained from the nocturnal flux observations above the canopy, separated into canopy and soil components. The total canopy conductance was also summed up layer by layer and delivered to use in other flux modules. In non-forested but still active regions (class 4 in Table 1) CO_2 exchange rates were obtained directly from chamber measurements.

Water vapour exchange was simulated by the Penman-Monteith formulation (see Appendix A). The potential evapotranspiration rate was used because there usually are no drought effects observable at the site and previous days had been rainy. Atmospheric resistance to water vapour transport was obtained from the radiation balance calculations and the total canopy resistance from CO_2 exchange model. The gas exchange module together with heat flux and transport equations thus formed a closely linked system, where changes in one module altered results of other components.

3. Results

3.1. Flow patterns and CO_2 profiles

Simulations were first performed for near-optimal summer midday conditions, i.e. for 22 July 1998, when temperature was around 17°C at the flux measurement site according to measurements, and cloudless sky provided optimal irradiance conditions. Prevailing moderate (~3–4 m/s at flux site, ~8–9 m/s at hill top) winds arrived to site from the north-east direction.

The modeled wind direction changed moderately when moving from the boundary

to the forest (flux) site and the hill top (concentration) site due to topography-induced changes in wind speed and flow patterns. Model showed 51° for the forest site and 70° for the hill site, counted clockwise from north, while the wind direction at the boundary was about 47–57° at corresponding altitudes. The measurements showed a similar change from 38° to 78° when moving from forest site to hill site. The influence of heating of the surface was not important for the major flow patterns. Particles released from the ground surface and from the lateral boundary of the model at different altitudes showed the path of air parcels before they reached the hill top. The upwind path extended to northeast in current wind conditions, showing contributions from land cover classes c4 (46%), c3 (31%), c2 (19%) and c1 (4%). Examining further the vertical direction, particles released at 400–500 m height from the model boundary reached the hill top, situated 565 m a.s.l.

When the wind direction changes, also the vertical profiles of the species transferring in the air masses change, if the species have diverse sources and sinks in the surroundings of the observation point. At the hill site vertical profiles of CO_2 were studied when air flowed from north, south, east and west, respectively. Only wind direction at boundaries changed, all other boundary conditions were kept constant during the experiment including the lateral input profile of CO_2. The chain of hills extends mainly in north-south direction. When air masses arrived from east, first traveling over the plateau (and flux tower) and then to hill top, a profile of CO_2 was observed where lowest concentrations were found near the ground (Fig. 2). When air masses arrived from west the result was similar, but the profile was shifted to lower concentrations. Results for south and north were quite similar to east, north showing the highest concentrations near the ground. All profiles were rather close to each other showing less than 0.5 ppm difference at the lowest level, indicating the dominance of the boundary input. Generally the concentrations changed less than 15 ppm from ground to 3000 m. The northern and southern flows over the chain of hills resulted in concentration differences of similar magnitude than those caused by eastern flow over the plateau, while western flows were clearly different. Upwind paths showed that there were high productivity

ACPD
5, 10019–10053, 2005

land classes in greater proportion in west (Table 2) than in other directions. In north there were more low productivity land use classes. Thus, it seems that land use rather than topography creates the differences between the profiles. The topography had some effect, for example crossing the hill added more twists on the downwind potential temperature profile between 700 m and 1400 m altitude. However, midday CO_2 was relatively similar (<0.15 ppm) at both sides of the hill.

There exists a small sink of CO_2 at the hill top due to mosses, lichens and small sedges that grow in the rocky ground. Chamber measurements showed the sink to be about 0.2 μmol/m2s at maximum. This small flux, less than 2% of the assimilation rates measured at the forest site, may have an effect on the observed CO_2 concentration since it is close to the observation point which was located 10 m above ground. The effect of the sink was investigated by doubling the flux at the hill top in the simulations and comparing the result to the basic case with actual boundary wind fields (Fig. 3). The change in the flux resulted in a very small change in the CO_2 profile, decreasing the concentration at the lowest level by less than 0.1 ppm when using the higher flux. In reality the fluxes are probably even smaller than 0.4 μmol/m2s tested in the simulation, and thus the effects on the observed concentration can be neglected.

3.2. Diurnal development

Diurnal variation of the boundary layer height is important for observations of CO_2 concentration. If the measurement point is located inside a shallow inversion layer, the concentrations are not well mixed and may not be considered as regionally representative. At Pallas some indications of daily boundary layer development could be seen, although sun was less than three hours below horizon during that time of summer. Richardson number and potential temperature profiles were calculated for forest and hill top sites, and the boundary layer height was determined from the altitude where Ri rapidly increased (see e.g. Vogelezang and Holtslag, 1996), and there was a distinct change in potential temperature profile. The upper limit of the boundary layer was at about 100 m above fores site at night and gradually increased to about

900 m a.s.l. at 15:00 LT (= local time, UTC+3). The values are typical for the region (Aalto et al., 2002). The hills changed the boundary layer structure moderately, creating about 150 m difference in boundary layer height between forest and hill top sites.

Diurnal profiles of CO_2 were significantly different at the hill top site and at the forest site (Fig. 4). The original boundary input from a regional model with smaller vertical resolution is shown in the same figure, indicating that the profiles at hill top follow the boundary forcing quite closely, while concentrations at forest site deviate at the lowest levels. During night the lowest level concentrations at the forest site were about 2 ppm higher than at the hill top. At night the inversion layer was less than hundred meters above the forest site. Between 06:00 and 07:00 LT respiration turned into assimilation and the lowest level CO_2 concentration decreased to near hill top values. At 15:00 LT forest site concentrations were about 5 ppm lower than hill top values. Later during the afternoon concentrations at the forest site started to increase and between 19:00 and 20:00 LT they increased to values higher than concentrations at hill top.

The same diurnal cycle can be seen in Fig. 5, where lowest level concentrations at hill top and forest site are shown together with boundary forcing and measured concentrations. Concentration observations from eddy covariance system at the flux tower at the forest site were not as accurate as measurements at the hill top (about 3 ppm measurement accuracy vs. 0.1 ppm), but the diurnal cycle with an amplitude of about 28 ppm could easily be distinguished from the background. At the hill top the diurnal variation was only 9 ppm. A large difference between lower and higher altitude measurements is quite typical for a site with local sinks (see e.g. Denning et al., 2003). According to simulations, the diurnal variation at the forest site was only 10 ppm and at hill top 4 ppm. Simulation followed the boundary forcing very closely at the hill top but not at the forest site. Diurnal cycle was not very clear in the boundary input, resulting from a 1.5 ppm decrease in the oceanic component in the morning (between 07:00 and 10:00 LT) and a small increase of 1 ppm in anthropogenic component in the afternoon (between 15:00 and 18:00 LT). Both elevated the composite concentration while the biospheric component acted in opposite direction. The biospheric component showed

ACPD
5, 10019–10053, 2005

a diurnal cycle of 4.3 ppm, which is less than the measured diurnal variation.

Both model and measurements indicated a small increase in CO_2 concentrations at 10:00 LT. The night time CO_2 release by respiration had already turned into assimilation by that time, and concentrations inside the inversion layer were in average lower than above the layer. The increase according to measurements at the forest site most probably resulted from a small temporary drawdown in CO_2 fluxes. The increase in the modeled values was probably due to the corresponding modeled flux drawdown together with boundary input, which also showed a small increase at 10:00 LT. To clarify the role of boundary layer development and mixing procedure, a simulation with an inert tracer (^{222}Rn) with constant release from the ground was performed (e.g. Chevillard et al., 2002; see also Betts et al., 2004). The results did not show any sudden changes in concentration during the morning, which would suggest effects by boundary layer dynamics. However, contours of CO_2 in a model cross section at 12:00 LT (Fig. 6) varied with altitude. CO_2 profiles were smooth above the inversion and there was more vertical and small scale horizontal variation inside the boundary layer. At the ground level there was considerable variation in CO_2 concentrations and fluxes from one grid cell to another due to the variability of the surface fluxes. Rn concentrations were less variable than CO_2due to smooth source distribution.

3.3. CO_2 fluxes

Measured fluxes of CO_2 showed a daily maximum at 12:00 LT at the forest site (Fig. 7). Net assimilation turned positive between 06:00 and 07:00 LT. The daily maximum of CO_2 flux was about two to three hours out of phase from the concentration cycle, showing the delayed response of concentrations to the flux signal. This was not seen in the model results, where concentrations followed closely flux development and boundary input with distinct afternoon increase. Simulated flux values were similar to measured fluxes showing daily maximum at 13:00 LT and slightly higher values during early afternoon. This happened because the model predicted relative humidity of about 70% due to boundary input while measurements indicated *RH* of only about 50% at 13:00–

16:00 LT. As a consequence, the modeled canopy conductance stayed rather constant until late afternoon allowing high CO_2 assimilation rates while the measured rates were depleted already during earlier hours in spite of favorable irradiance and temperature conditions. Modeled canopy resistance for water vapor was about 100 m/s and atmospheric resistance 15 m/s during the active daylight hours. Latent and sensible heat fluxes followed measurements (Fig. 8), showing a rapid decrease during early evening when stability conditions changed from near-neutral towards unstable stratification according to eddy system readings. During last two hours modeled and experimental CO_2 fluxes differed considerably probably because of the change in stability conditions and low friction velocity making the flux measurement uncertain.

The average assimilation rate for the whole model domain of 10×10 km was calculated from the model results, which provided individual flux values for each 50×50 m grid cell. The average rate for the whole region (Fig. 9) was roughly 55–60% smaller than the modeled flux at eddy covariance site, resulting from the location of the flux site in a dense forest of the highest flux class in the model domain. The percentages were slightly higher during night, and thus caution must be taken when generalizing the result over long time periods. The timing and shape of the diurnal cycle of the average flux was very similar to the cycle at the flux site. The net flux, i.e. sum of all cells in the domain, was 19 kg(CO_2) s^{-1} at 13:00 LT, which was the highest value during the day, and the sum over the whole day was 0.12 Gg(CO_2). For the forest site the highest flux of 0.47 mg(CO_2) m^{-2} s^{-1} was modeled at 13:00 LT, and the sum over the whole day was 8.4 g(CO_2) m^{-2}. If the fluxes at the forest site are simply generalized to apply to every grid cell in the whole model domain, then the net daily result for the whole region would be 0.84 Gg(CO_2), which gives a large overestimation in comparison to the simulated net flux of 0.12 Gg(CO_2). A simulation of CO_2 concentrations with these large fluxes showed, that the concentration at the hill top would decrease by 0.5 ppm. The change in profile could be seen from surface to 1000 m a.s.l. altitude. Ambient conditions at the flux site were, however, quite similar to other forested areas in the region. When the vegetation flux submodel was applied to the whole region using flux

site reference values instead of those given individually for each grid cell by the atmospheric model, the obtained CO_2 fluxes for the region were in 15% of the 3-D model result.

4. Discussion and conclusions

In general, topography and different sink patterns along the flow direction induce changes in flow and concentration patterns. Here the CO_2 profile changed moderately (<0.5 ppm) at the hill top after changes in wind direction. The main reason for the profile change was the difference in vegetation sink upwind from the site, rather than topology. Smallest concentrations were observed when air masses arrived from west, western upwind path having largest CO_2 fluxes. During northern winds the air flowed over a chain of hills resulting in slightly higher lowest level concentrations, and showing thus the effect of low assimilation rates at non-forested hill tops on the CO_2 profile. The small sink at the hill site due to assimilation by mosses and lichens did not have a significant effect on the observed concentration.

The profile at the concentration measurement site followed closely the boundary conditions, indicating good possibilities to observe long range transported CO_2 signals at Pallas site (see Aalto et al., 2002; Eneroth et al., 2005). This was not the case at the forest site (however, see Potosnak et al., 1999, for using suitable correlates to obtain representative concentrations near canopy). During night respiration elevated the concentration values at the forest site, and during daytime the closely located sinks lowered the concentration by about 5 ppm in comparison to the boundary input. Moving higher up in the troposphere, the concentrations reached the hill top values at about 60–100 m above surface at midday conditions. The model could not simulate the measured diurnal amplitude at the forest site. At the hill site the agreement with measurements was better, though dominated by the boundary input which included some long range transported features that were not observed in the measurements. High concentrations during night were especially difficult to simulate at the forest site. This

ACPD
5, 10019–10053, 2005

may result from low mixing layer height, low wind speeds and canopy structure creating turbulence patterns that can not be reproduced with the current model, which does not include trees as separate objects. Afternoon concentration values were, however, in good agreement with the measurements and also the difference between hill top and forest site was similar according to model and measurements.

The modeled fluxes agreed with the measured fluxes at the forest site. The average flux to the total model domain was lower than the flux at the forest site, owing to the high productivity of the flux site. If the flux at the forest site is used for the whole model area, an overestimation is always obtained. If these large fluxes are used to simulate concentration profiles, they will be distorted. For coarse resolution studies it would therefore be useful to scale the fluxes from site to region using a vegetation model together with land use information, if a local scale atmospheric model is not available.

The aim of the continuous measurements at Pallas is to study Northern Scandinavian scale atmospheric CO_2 signal reliably. According to current results, measurements are representative for continental background at the hill top, as well as high above vegetation, whether in upwind or downwind side of the hills. Due to boundary layer development, air parcels observed at the hill top are coupled with the local surface during daytime and separated during night. The input from model lateral boundaries was dominant in both cases. According to different tests, the local vegetation and topography changed the concentrations less than 0.6 ppm. It can be concluded that in view of the current results the location of the site provides good possibilities for achieving the measurement aims. More generally, it is possible to perform representative measurements at vegetated hills and above active forest, provided vertical distance to sinks is sufficient.

ACPD
5, 10019–10053, 2005

Appendix A

The radiation balance of the ground surface may be written as follows (e.g. Hartmann, 1994):

$$R = LE + SH + G \tag{A1}$$

where LE is latent heat flux, SH is sensible heat flux, G is ground heat flux and R is the absorbed net radiation. Combining vegetation and ground heat fluxes, the total latent heat flux can be written as

$$LE = -\frac{\rho_1 c_p}{\gamma}\frac{(e_1 - e_s)}{r_{aw}} \tag{A2}$$

where ρ_1 is the air density at lowest model level above surface, c_p is the specific heat of the air, γ is the psychrometric constant (Pa/K), e_1 is the water vapor pressure at the lowest model level and e_s at the surface. r_{aw} is the aerodynamic resistance (s/m) for water vapour transfer between the lowest model level and surface, given by

$$r_{aw} = \frac{1}{k^2 v_1}\left[\ln\left(\frac{z_1 - d}{z_{0m}}\right) - \Psi_m(\zeta)\right]\left[\ln\left(\frac{z_1 - d}{z_{0w}}\right) - \Psi_w(\zeta)\right] \tag{A3}$$

where k is von Karman constant (0.4), v is wind speed, z_1 is the height of the first model level, d is displacement height, z_{0m} roughness length for momentum, z_{0h} roughness length for heat, ζ atmospheric stability and $\Psi(\zeta)$ Monin-Obukhov similarity functions (Kaimal and Finnigan, 1994), which increase the resistance in stable conditions and decrease in unstable conditions. Total sensible heat flux can be written as

$$SH = -\rho_1 c_p \frac{(\theta_1 - T_s)}{r_{ah}} \tag{A4}$$

Where θ is potential temperature at the lowest model level and T_s is the surface temperature. r_{ah} is calculated analogously to r_{aw}. G is the ground heat flux, which is estimated to be 3.6% of the net radiation (Verma et al., 1986).

ACPD
5, 10019–10053, 2005

Net radiation R can be further divided into shortwave (SW) and longwave (LW) components, and expressed by means of SW and LW downward fluxes as follows:

$$R = SW_{\text{down}}(1 - a) + \varepsilon \left(LW_{\text{down}} - \sigma T_s^4 \right) \tag{A5}$$

where a is SW albedo of the surface, ε is LW emissivity of the surface and σ is the Stefan-Bolzmann constant. a and ε were obtained from Modis satellite results for Pallas/Kenttärova (http://www.modis.ornl.gov/modis/). $SW+LW$ downward fluxes were obtained from local radiation measurements. Total potential global radiation at the surface was modeled according to Savijärvi (1990). LW radiation absorption in the atmosphere was calculated including water vapour as the absorbing substance and applying methods by Chou (1992).

Potential evapotranspiration was calculated using the Penman-Monteith equation (Monteith and Unsworth, 1990):

$$\lambda E = \frac{\Delta (R - G) + \rho_1 c_p \frac{(e_s - e_1)}{r_{aw}}}{\Delta + \gamma \left(1 + \frac{r_{cw}}{r_{aw}} \right)} \tag{A6}$$

where Δ represents the slope of the saturation vapour pressure vs. temperature relationship and r_{aw} is the bulk aerodynamic resistance for water vapour transfer and r_{cw} is the canopy resistance for water vapour transfer. r_{aw} is obtained from Eq. (3) and r_{cw} is obtained from CO_2 transport simulations explained below.

CO_2 assimilation rates were first calculated at leaf level by finding the minimum of the RuBP regeneration-limited net CO_2 exchange rate (A_j) and net Rubisco-limited CO_2 exchange rate (A_c), as introduced by Farquhar et al. (1980) and DePury and Farquhar (1997):

$$A_j = J \frac{c_i - \Gamma_*}{4 (c_i + 2\Gamma_*)} - R_d \tag{A7}$$

ACPD
5, 10019–10053, 2005

$$A_c = V_{c(\max)} \frac{c_i - \Gamma_*}{k_c\left(1 + o/k_o\right) + c_i} - R_d \tag{A8}$$

where $V_{c(\max)}$ is the maximum rate of carboxylation, J is the potential electron transport rate, R_d is the rate of non-photorespiratory respiration, k_c and k_o are the Michaelis-Menten constants, Γ_* is the CO_2 compensation point in the absence of non-photorespiratory respiration, o is the oxygen concentration in chloroplasts (assumed constant) and c_i is here the local carbon dioxide concentration inside forest, connected to ambient concentration through r_{aw}. J can be written as

$$J = \frac{qI_0 + J_{\max} - \sqrt{(qI_0 + J_{\max})^2 - 4\Theta qI_0 J_{\max}}}{2\Theta} \tag{A9}$$

Where (I_0) is the incident irradiance, Θ is convexity factor, q is light use effectivity factor and $J_{\max}$ is the maximum electron transport rate. $J_{\max}$, $V_{c(\max)}$ and q were obtained from Scots pine studies in northern Finland (Aalto, 1998; Thum et al., 2005[1]). Leaf respiration rates were obtained from leaf chamber respiration measurements conducted in Sodankylä, northern Finland (Thum et al., 2005[1]). Other parameter values and their temperature dependencies were taken from literature (see Aalto and Juurola, 2002).

Conductances were calculated using the following equation (Ball et al., 1987)

$$g = g_0 + g_l \frac{Ae_1/e_{\text{sat}}}{c} \tag{A10}$$

Where g_0 (2.8) and g_l (0.027) are empirical coefficients fitted to the Pallas flux data.

Leaf level assimilation rates and conductances were calculated for each four vertical layers in the canopy. The canopy biomass was assumed to be distributed according to beta distribution, as presented for Scots pine by Wu et al. (2003), and incident diffuse

[1]Thum, T., Aalto, T., Aurela, M., Laurila, T., Kolari, P., and Hari, P.: Seasonal development of CO_2 exchange model parameters obtained by inverting canopy models, in preparation, 2005.

and direct irradiance in each layer was simulated according to a two-flux irradiance model (Sellers, 1985; Sellers et al., 1996). Assimilation rates and conductances were calculated separately for sunlit and shaded portions of LAI (e.g. Thornley, 2002). $V_{c(\max)}$ and $J_{\max}$ were assumed to decrease exponentially inside canopy (Dang et al., 1997):

$$V_{c\max} = V_{c\max t} \frac{LAI_{\text{tot}}}{k_d D} \left(1 - \exp\left[-k_d D\right]\right) \quad \text{(A11)}$$

Where k_d is extinction coefficient for light, d is depth into canopy and LAI_{tot} the total leaf area index of the canopy, measured at the site.

Finally, results for the layers were summed up together to obtain the canopy conductance, CO_2 assimilation rate and respiration rate. Soil respiration rate was solved from the net ecosystem respiration from nighttime eddy covariance measurements, and added to the result. Canopy conductance was transformed to water vapour resistance (r_{cw}) and used in heat and water vapour transport calculations.

Acknowledgements. The authors would like to acknowledge the CARBOEUROPE-IP project (EVK2-CT-1999-00032), and fruitful co-operation with Finnish Forest Research Institute, Pallas-Ounastunturi National Park and Finnish Land Survey.

References

Aalto, T. and Juurola, E.: Parametrization of a biochemical CO_2 exchange model for birch (*Betula pendula* Roth.), Boreal Environ. Res., 6, 53–64, 2002.

Aalto, T.: Carbon dioxide exchange of Scots pine shoots as estimated by a biochemical model and cuvette field measurements, Silva Fennica, 32(4), 321–337, 1998.

Ball, J. T., Woodrow, I. E., and Berry, J. A.: A model predicting stomatal conductance and its contribution to the control of photosynthesis under different environmental conditions, in: Progress in Photosynthesis Research, edited by: Biggins, J. and Nijhoff, M., 4, 221–224, 1987.

Beljaars, A. C. M. and Holtslag, A. A. M.: Flux parametrization over land surfaces for atmospheric models, J. Appl. Meteorol., 30, 327–341, 1991.

Betts, A. K., Helliker, B., and Berry, J.: Coupling between CO_2, water vapour, temperature, and radon and their fluxes in an idealized equilibrium boundary layer over land, J. Geophys. Res., 109, D18103, doi:10.1029/2003JD004420, 2004.

Carvalho, J. C., Anfossi, D., Castelli, T., and Degrazia, G. A.: Application of a model system for the study of transport and diffusion in complex terrain to the TRACT experiment, Atmos. Environ., 36, 1147–1161, 2002.

Chan, D., Yuen, C. W., Higuchi, K., Shashkov, A., Liu, J., Chen, J., and Worthy, D.: On the CO_2 exchange between the atmosphere and the biosphere: the role of synoptic and mesoscale processes, Tellus, 56B, 194–212, 2004.

Chevillard, A., Karstens, U., Ciais, P., Lafont, S., and Heimann, M.: Simulation of atmospheric CO_2 transport in Europe and Siberia using the regional scale model REMO, Tellus, 54B, 872–895, 2002.

Chou, M. D.: A solar radiation model for use in climate studies, J. Atmos. Sci., 49(9), 762–772, 1992.

Dang, Q. L., Margolis, H. A., Sy, M., Coyea, M. R., Collatz, G. J, and Walthall, C. L.: Profiles of photosynthetically active radiation, nitrogen and photosynthetic capacity in the boreal forest: Implications for scaling from leaf to canopy, J. Geophys. Res., 102(D24), 28 845–28 859, 1997.

Dargaville, R. J., Heimann, M., McGuire, A. D., Prentice, I. C., Kicklighter, D. W., Joos, F., Clein, J. S., Esser, G., Foley, J., Kaplan, J., Meier, R. A., Melillo, J. M., Moore III., B., and Ramankutty, N.: Evaluation of terrestrial carbon cycle models with atmospheric CO_2 measurements: Results from transient simulations considering increasing CO_2, climate, and land-use effects, Global Biogeochem. Cycles, 16(4), 1092, doi:10.1029/2001GB001426, 2002.

Denning, S., Nicholls, M., Prihodko, L., Baker, I., Vidale, P.-L., Davis, K., and Bakwin, P.: Simulated variations in atmospheric CO_2 over a Wisconsin forest using a coupled ecosystem-atmosphere model, Global Change Biology, 9, 1241–1250, 2003.

DePury, D. G. G. and Farquhar, G. D.: Simple scaling of photosynthesis from leaves to canopies without the errors of big-leaf models, Plant, Cell Environ., 20, 537–557, 1997.

Farquhar, G. D., von Caemmerer, S., and Berry, J. A.: A biochemical model of photosynthetic CO_2 assimilation in leaves of C3 species, Planta, 149, 78–90, 1980.

Gangoiti, G., Alonso, L., Maruri, M., Navazo, M, and Pérez-Landa, G.: UHF Radar Detection and Numerical Simulation of an Episode of Foehn and Lee Waves over the Northern Coast of Iberia, J. Appl. Meteorol., 41(3), 230–240, 2002.

ACPD

5, 10019–10053, 2005

Geels, C., Doney, S. C., Dargaville, R., Brandt, J., and Christensen, J. H.: Investigating the sources of synoptic variability in atmospheric CO_2 measurements over the Northern Hemisphere continents: a regional model study, Tellus, 56B, 35–50, 2004.
Gloor, M., Bakwin, P., Hurst, D., Lock, L., Draxler, R., and Tans, P.: What is the concentration footprint of a tall tower?, J. Geophys. Res., 106(D16), 17 831–17 840, 2001.
Grell, G. A., Emeis, S., Stockwell, W. R., Schoenenmayer, T., Forkel, R., Michalakes, J., Knoche, R., and Seidl, W.: Application of a multiscale, coupled MM5/chemistry model to the complex terrain of the VOTALP valley campaign, Atmos. Environ., 34, 1435–1453, 2000.
Gurney, K. R., Law, R. M., Denning, A. S., Rayner, P. J., Pak, B. C, Baker, D., Bousquet, P., Bruhwiler, L., Chen, Y. H., Ciais, P., Fung, I. Y., Heimann, M., John, J., Maki, T., Maksyutov, S., Peylin, P., Prather, M., and Taguchi, S.: Transcom 3 inversion intercomparison: Model mean results for the estimation of seasonal carbon sources and sinks, Global Biogeochem. Cycles, 18, doi:10.1029/2003GB002111, 2004.
Hartmann, D. L.: Global Physical Climatology, Academic Press, San Diego, USA, 408 pp., 1994
Henne, S., Furger, M., Nyeki, S., Steinbacher, M., Neininger, B., de Wekker, S. F. J., Dommen, J., Spichtinger, N., Stohl, A., and Prevot, A. S. H.: Quantification of topographic venting of boundary layer air to the free troposphere, Atmos. Chem. Phys., 4, 497–509, 2004, SRef-ID: 1680-7324/acp/2004-4-497.
Hatakka, J., Aalto, T, Aaltonen, V., Aurela, M., Hakola, H., Komppula, M., Laurila, T., Lihavainen, H., Paatero, J., Salminen, K., and Viisanen, Y.: Overview of atmospheric research activities and results at Pallas GAW station, Boreal Environ. Res., 8, 365–384, 2003.
Houweling, S., Dentener, F., Lelieveld, J., Walter, B., and Dlugokencky, E.: The modeling of tropospheric methane: How well can point measurements be reproduced by a global model?, J. Geophys. Res., 105(D7), 8981–9002, 2000.
Kaimal, J. C. and Finnigan, J. J.: Atmospheric boundary layer flows, Oxford University Press, New York, USA, 289 pp., 1994
Knorr, W. and Heimann, M.: Uncertainties in global terrestrial biosphere modeling, part II: Global constraints for a process-based vegetation model, Global Biogeochem. Cycles, 15(1), 227–246, doi:10.1029/1998GB001060, 2001.
Kjellström, E., Holmen, K., Eneroth, K., and Engardt, M.: Summertime Siberian CO_2 simulations with the regional transport model MATCH: A feasibility study of carbon uptake calculations from EUROSIB data, Tellus, 54B, 834–849, 2002.

Monteith, J. L. and Unsworth, M.: Principles of Environmental Physics, Butterworth-Heinemann, Oxford, GB, 291 pp., 1990.

Potosnak, M. J., Wofsy, S., Denning, A. S., Conway, T. J., Munger, J. M., and Barnes, D. H.: Influence of biotic exchange and combustion sources on atmospheric CO_2 concentrations in New England from observations at a forest flux tower, J. Geophys. Res., 104(D8), 9561–9569, 1999.

Ramonet, M. and Monfray, P.: CO_2 baseline concept in 3-D atmospheric transport models, Tellus, 48B, 502–521, 1996.

Rannik, Ü., Aubinet, M., Kurbanmuradov, O., Sabelfeld, K. K., Markkanen, T., and Vesala, T.: Footprint analysis for measurements over a heterogeneous forest, Boundary Layer Meteorol., 97, 137–166, 2000.

Rao, K. S. and Nappo, C. J.: Turbulence and dispersion in the stable atmospheric boundary layer, in: Dynamics of the Atmospheric Flows: Atmospheric Transport and Diffusion Processes, edited by: Singh, M. P. and Raman, S., Computational Mechanics Publications, 39–91, 1998.

Rebmann, C., Göckede, M., Foken, T., Aubinet, M., Aurela, M., Berbigier, P., Bernhofer, C., Buchmann, N., Carrara, A., Cescatti, A., Ceulemans, R., Clement, R., Elbers, J. A., Granier, A., Grünwald, T., Guyon, D., Havrankova, K., Heinesch, B., Knohl, A., Laurila, T., Longdoz, B., Marcolla, B., Markkanen, T., Miglietta, F., Moncrieff, J., Montagnani, L., Moors, E., Nardino, M., Ourcival, J. M., Rambal, S., Rannik, Ü., Rotenberg, E., Sedlak, P., Unterhuber, G., Vesala, T., and Yakir, D.: Quality analysis applied on eddy covariance measurements at complex forest sites using footprint modeling, Theor. Appl. Climatol., 80(4), 121–141, doi:10.1007/s00704-004-0095-y, 2005.

Savijärvi, H.: Fast radiation parametrization schemes for mesoscale and short-range forecast models, J. Appl. Meteorol., 29, 437–447, 1990.

Sellers, P. J.: Canopy reflectance, photosynthesis and transpiration, Int. J. Remote Sens., 6, 1335–1372, 1985.

Sellers, P. J., Randall, D. A., Collatz, G. J., Berry, J. A., Field, C. B., Dazlich, D. A., Zhang, C., Collelo, G. D., and Bounoua, L.: A revised land surface parametrization (SiB2) for Atmospheric GCMs. Part I: Model formulation, J. Clim., 9, 676–705, 1996.

Sogachev, A., Menzhulin, G. V., Heimann, M., and Lloyd, J.: A simple three-dimensional canopy – planetary boundary layer simulation model for scalar concentrations and fluxes, Tellus, 54B, 784–819, 2002.

ACPD

5, 10019–10053, 2005

Sogachev, A., Panferov, O., Gravenhorst, G., and Vesala, T.: Numerical analysis of flux footprints for different landscapes, Theor. Appl. Climatol., 80(4), 169–185, doi:10.1007/s00704-004-0098-8, 2005.

Troen, I. and Petersen, E. L.: European Wind Atlas, Risø National Laboratory, Roskilde, 656 pp., 1989.

Thornley, J. H. M.: Instantaneous canopy photosynthesis: Analytical expressions for sun and shade leaves based on exponential light decay down the canopy and an acclimated non-rectangular hyperbola for leaf photosynthesis, Annals of Botany, 89, 451–458, 2002.

Turner, D. P., Dodson, R., and Marks, D.: Comparison of alternative resolutions in the application of a spatially distributed biogeochemical model over a complex terrain, Ecological Modelling, 90, 53–67, 1996.

Vesala, T., Rannik, Ü., Leclerc, M., Foken, T., and Sabelfeld, K.: Flux and concentration footprints, Agr. Forest Met., 127, 111–116, 2004.

Wieringa, J.: Updating the Davenport roughness classification, J. Wind Engin. Industr. Aerodyn., 41–44, 357–368, 1992.

Verma, S. B., Baldocchi, D. D., Anderson, D. E., Matt, D. R., and Clement, R. J.: Eddy fluxes of CO_2, water vapor and sensible heat over a deciduous forest, Boundary Layer Meteorol., 36, 71–91, 1986.

Vogelezang, A. A. M. and Holtslaag, D. H. P.: Evaluation and model impacts of alternative boundary-layer height formulations, Boundary Layer Meteorol., 81, 245–269, 1996.

Wu, Y., Brashers, B., Finkelstein, P. L., and Pleim, J. E.: A multilayer biochemical dry deposition model, 1. Model formulation, J. Geophys. Res., 108, 4013–4025, 2003.

Table 1. Land cover types defined in the model.

class	1	2	3	4	5	6
type	forest	forest	forest	lichens, mosses and sedges	open wetland	lake
Tree density m^3/ha	>102	52–101	<52			
Percentage of cover	4.1	35	25	26	4.7	5.5

ACPD
5, 10019–10053, 2005

Table 2. Percentage contributions of different land classes to upwind path from the hill-top site.

Wind direction/class	1	2	3	4	5	6
West	12	50	19	18	1.9	0
North	0	13	26	61	0.2	0
East	1.5	26	30	28	14	0
South	1.5	41	24	20	3.0	11

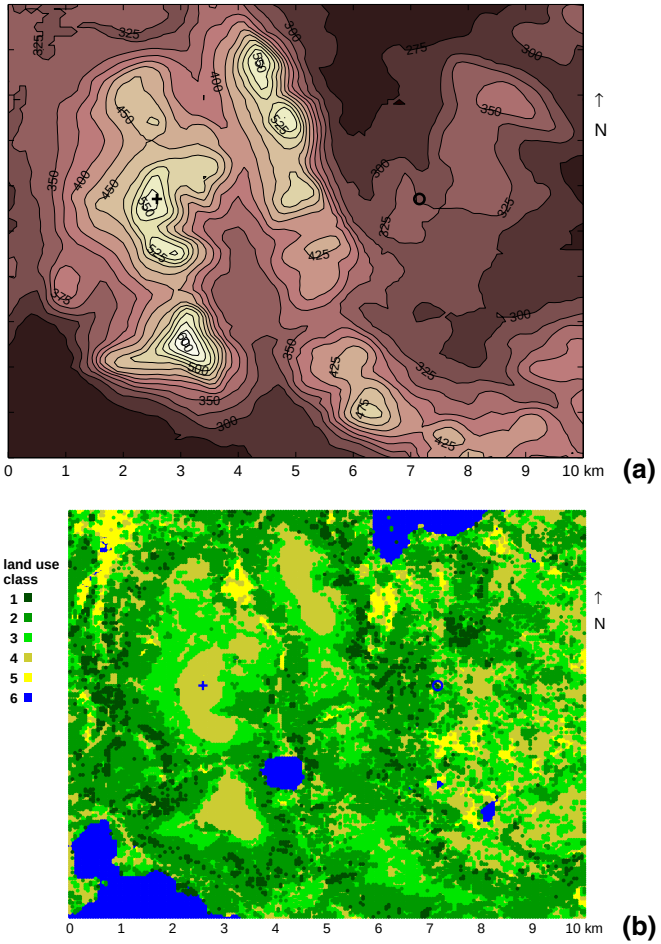

Fig. 1. Topography **(a)** and land use **(b)** in the 10×10 km model domain enclosing the Pallas measurement sites. The hill site is marked with a cross and the forest site with a circle.

ACPD

5, 10019–10053, 2005

Modeling CO_2 concentrations above sloping terrain

T. Aalto et al.

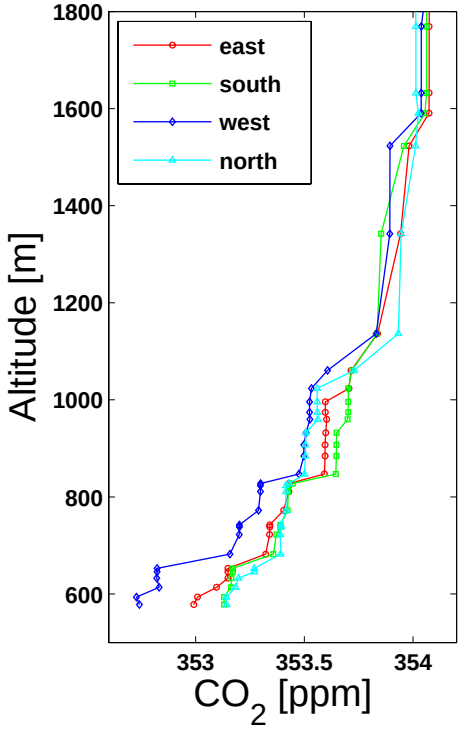

Fig. 2. Modeled CO_2 profiles at hill site when air masses come from the four main wind directions. Concentration values are shown in the center of each grid cell.

ACPD

5, 10019–10053, 2005

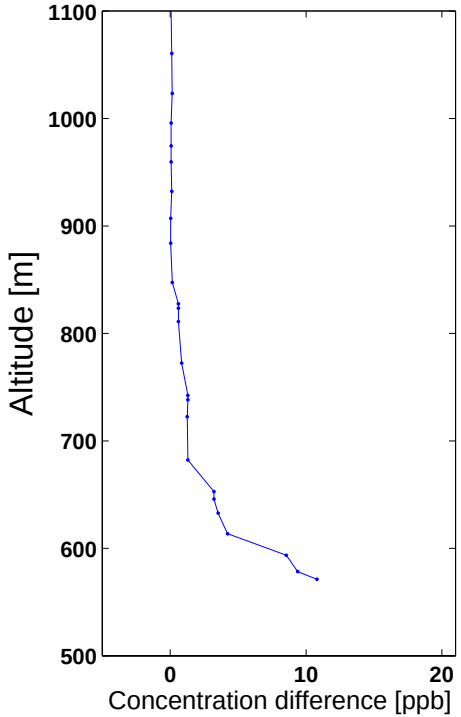

Fig. 3. Difference in modeled CO_2 profiles at hill site when the assimilation rate of ground vegetation is doubled. Lowest point is in the middle of the lowest model cell (11 m) near the actual measurement height (10 m).

ACPD

5, 10019–10053, 2005

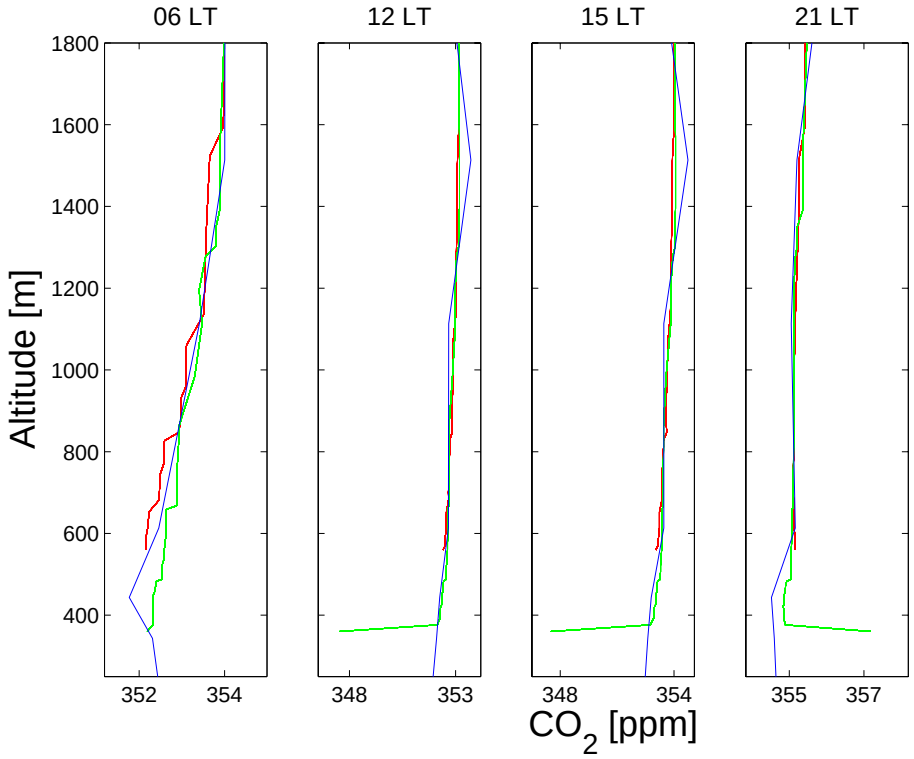

Fig. 4. Modeled profiles of CO_2 at hill site (red) and forest site (green), and boundary input (blue).

ACPD
5, 10019–10053, 2005

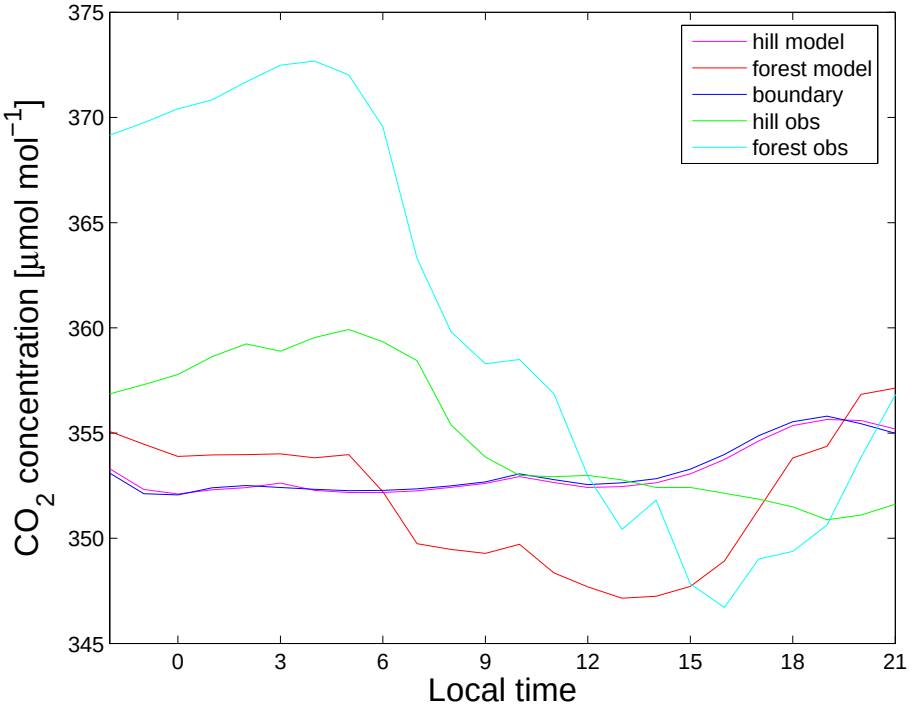

Fig. 5. Observed and modelled CO_2 concentrations at hill and forest sites together with input from model boundary.

ACPD
5, 10019–10053, 2005

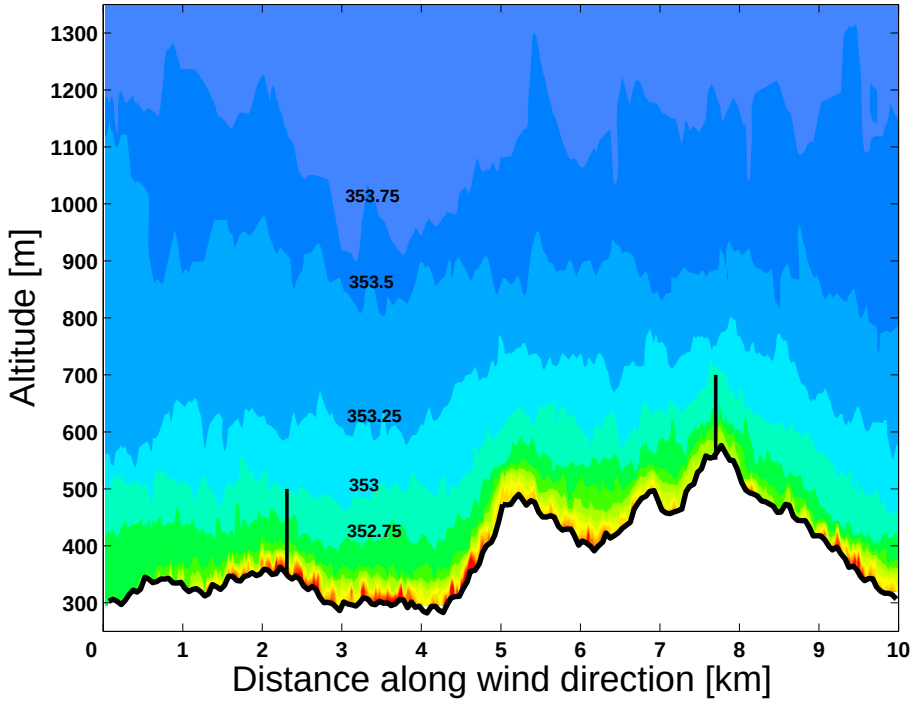

Fig. 6. CO_2 concentration contours in the cross section of the 3-D model pointed along direction of the air flow through the hill site. Vertical lines refer to locations of flux measurement site (lower left, projected to the plane) and the hill, or concentration measurement site (upper right). Concentration contours are plotted at 0.25 ppm intervals.

ACPD
5, 10019–10053, 2005

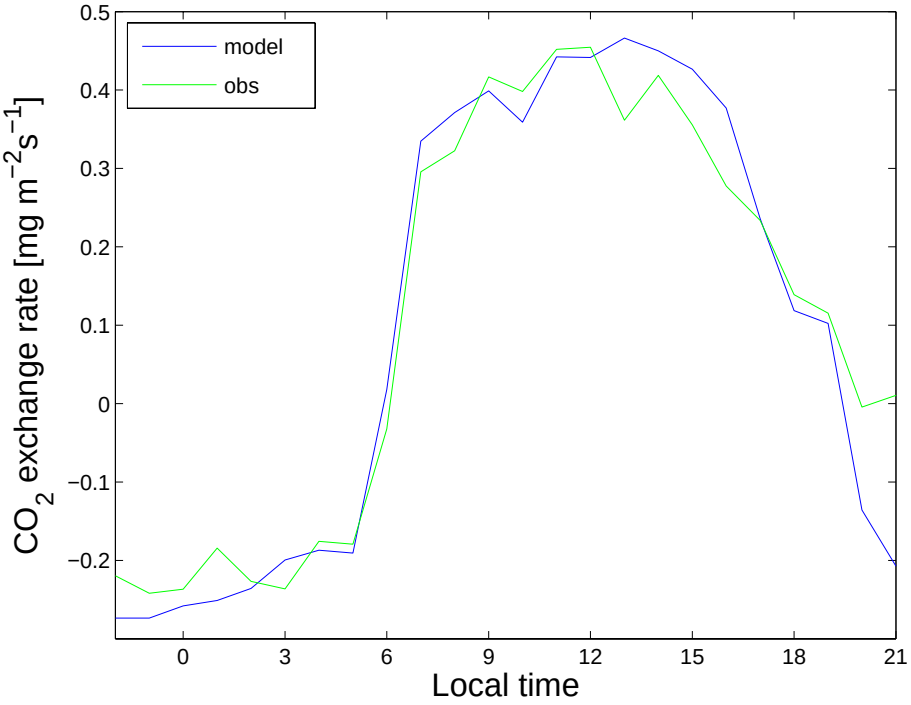

Fig. 7. CO_2 exchange rate at the forest site according to model and observations.

ACPD
5, 10019–10053, 2005

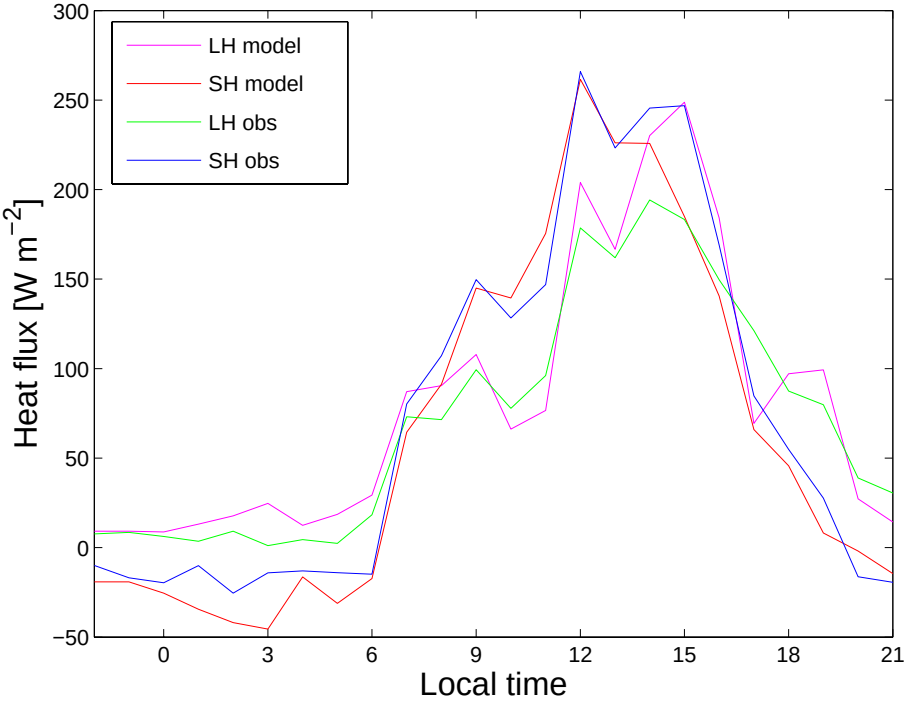

Fig. 8. Latent (LH) and sensible (SH) heat fluxes at the forest site according to model and observations.

ACPD
5, 10019–10053, 2005

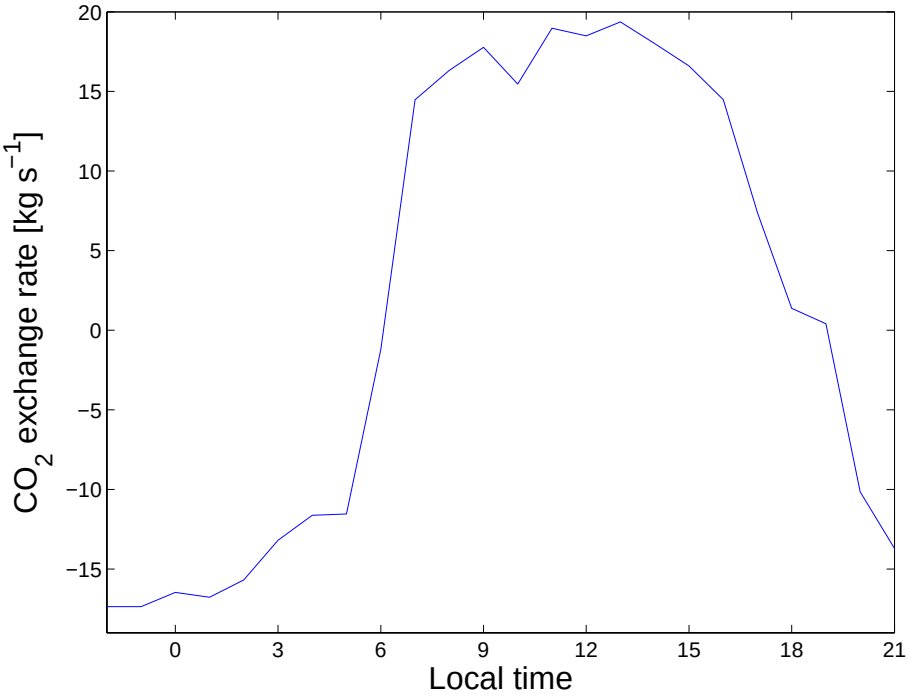

Fig. 9. CO_2 exchange rate for the 10×10 km model region.

ACPD
5, 10019–10053, 2005